Available online at www.sciencedirect.com
ScienceDirect
Earth and Planetary Science Letters 262 (2007) 468–483
EPSL
www.elsevier.com/locate/epsl

Time-dependent oxygen isotopic effects of CO self shielding across the solar protoplanetary disk

Edward D. Young

Department of Earth and Space Sciences and the Institute of Geophysics and Planetary Physics, University of California Los Angeles, 595 Charles E. Young Drive East, 2676 Geology, Los Angeles, CA 90095, United States

Received 25 March 2007; received in revised form 4 August 2007; accepted 6 August 2007
Available online 23 August 2007
Editor: R.W. Carlson

Abstract

Optically thin surfaces of the solar circumstellar disk were likely sites for generating ^{16}O isotope variability in the early Solar System. Astrochemical reaction network calculations predict that a robust feature of these photoactive horizons of the disk was conversion of CO gas to ^{16}O-poor (high $\Delta^{17}O$) H_2O ice on a timescale of 10^5 yr. Within several AU of the central star ultraviolet fluxes were too great for the oxygen isotopic effects of CO photodissociation to be sequestered in H_2O, meaning that the CO self shielding oxygen isotopic effect was an outer disk phenomenon. Calculations depicting transport in the circumstellar disk suggest that CO photodissociation at disk surfaces triggered a wave of high-$\Delta^{17}O$ H_2O that passed from surface regions through the outer disk and into the rocky planet-forming region on a timescale of 10^5 to 10^6 yr.

Keywords: oxygen isotopes; meteorites; photochemistry; CO self shielding

1. Introduction

The anomalous mass-independent distribution of $^{18}O/^{16}O$ and $^{17}O/^{16}O$ among rocky bodies is one of the most pronounced chemical features of the Solar System. Rock oxygen isotope ratios exhibit large variations in ^{16}O relative to both ^{17}O and ^{18}O (expressed as $\Delta^{17}O$[1]) rather than the expected mass-dependent trend in which fractional changes in $^{17}O/^{16}O$ are about half those in $^{18}O/^{16}O$. The cause of this anomalous behaviour among the isotopes of oxygen in primitive Solar System materials has remained a mystery since its discovery (Clayton et al., 1973).

Self shielding by CO, especially at low temperatures, is an attractive explanation for $\Delta^{17}O$ variability in the Solar System because it is a process observed to be going on in the interstellar medium and, perhaps, in disks as well (Brittain et al., 2005; Sheffer et al., 2002). It also has the advantage that a principle by-product is ^{16}O-depleted H_2O. The latter appears to be an important feature of the distribution of oxygen in the early solar nebula (Clayton and Mayeda, 1984; Young, 2001).

Here variations in oxygen isotope ratios in H_2O produced by CO self shielding as a function of position and time in the solar circumstellar disk are quantified

E-mail address: eyoung@ess.ucla.edu.

[1] Oxygen isotope ratios are written in terms of $\delta^{17}O$ and $\delta^{18}O$. These "delta" values refer to the per mil difference from the ratio in a reference reservoir j such that $\delta^iO = 10^3((^iO/^{16}O)/(^iO/^{16}O)_j - 1)$ where i refers to either 17 or 18. The reference reservoir j is either the Standard Mean Ocean Water (SMOW) reference for oxygen isotope measurements or the initial solar value used as an initial condition for the models. We will also refer to $\Delta^{17}O$ ("big delta ^{17}O"), usually defined as $\Delta^{17}O = \delta^{17}O - 0.52\,\delta^{18}O$. $\Delta^{17}O$ represents the degree of departure from mass-dependent fractionation relative to some reference reservoir of oxygen.

0012-821X/$ - see front matter © 2007 Elsevier B.V. All rights reserved.
doi:10.1016/j.epsl.2007.08.011

using reaction network calculations and a simple box model for transport in the disk. The result shows that isotope selective photodissociation of CO is likely to have been a hallmark of the outer solar circumstellar disk at distances from the star of > 5 AU, requiring transport of the anomalous oxygen isotope signal inward to the planet forming regions of the disk. Calculations show that this transport was in the form of a wave of high-$\Delta^{17}O$ water passing from the outer Solar System to the inner Solar System on a timescale of 10^5 to 10^6 yr.

2. CO photodissociation and self shielding

Carbon monoxide experiences destruction by photodissociation induced by far ultraviolet (FUV) stellar radiation at wavelengths of 91 to 110 nm. Photodestruction takes place primarily through predissociation. Predissociation involves passage to bound excited states prior to dissociation. Since the excited molecules have well-defined rovibrational states, photolysis by predissociation is isotope specific. The CO isotopologues $C^{16}O$, $C^{17}O$ and $C^{18}O$ will absorb FUV wavelengths in proportion to their column densities. Because typical $^{16}O/^{18}O$ and $^{16}O/^{17}O$ ratios in the interstellar medium and in envelopes around stars are ~ 250 to 600 and ~ 800 to 2600, respectively (Wilson, 1999), spectral lines for $C^{16}O$ will be more optically thick than $C^{17}O$ and $C^{18}O$ lines (van Dishoeck and Black, 1988). Saturation of the photodissociating lines of the abundant isotopologue is referred to as self shielding and is a process known to be important in the interstellar medium (ISM) (Bally and Langer, 1982; Sheffer et al., 2002).

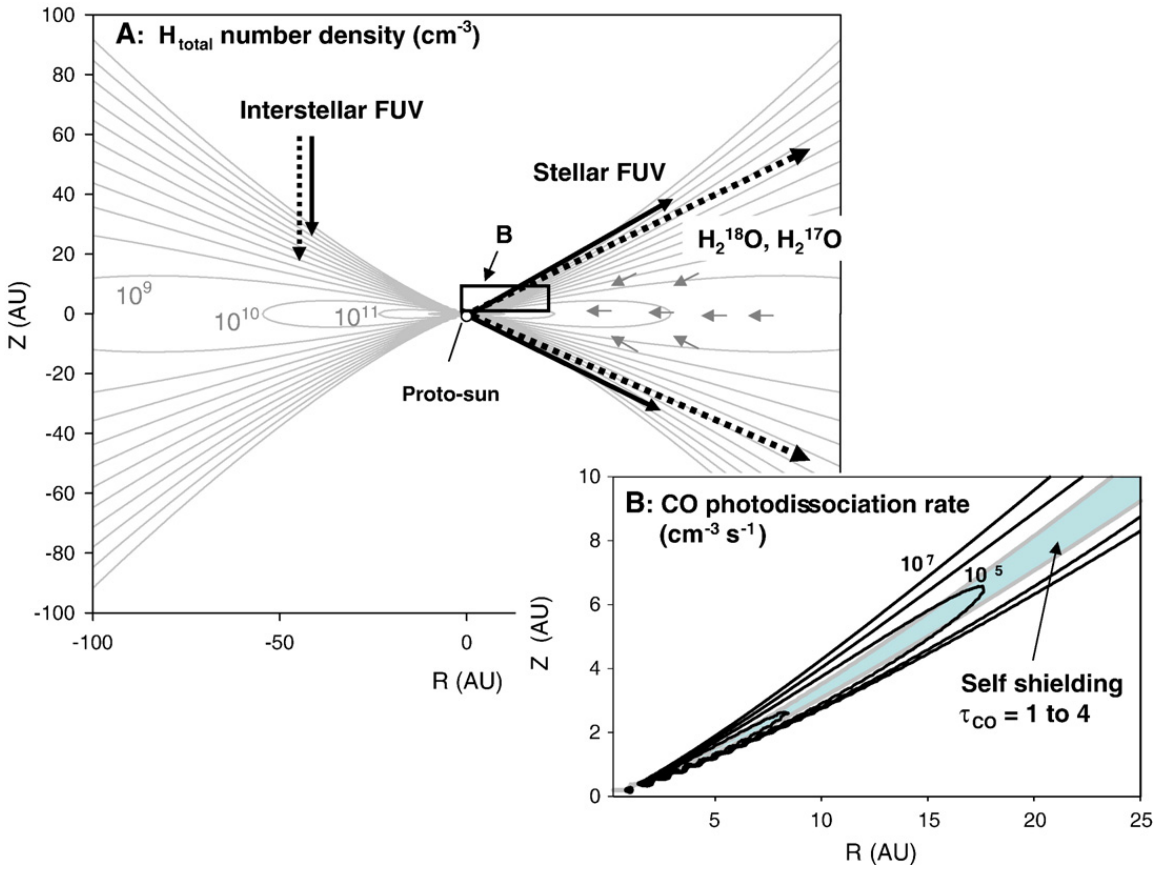

Fig. 1. Contour maps of the model circumstellar disk used in this study as viewed edge on. The disk model is the "Kyoto" model used to describe the accretion disk surrounding DM Tau (Aikawa and Herbst, 2001). The model is appropriate for a relatively evolved protoplanetary circumstellar disk. A: Grey contours show H nuclei number densities ($n(H_{tot})$), increasing inward towards the central star in single decade increments. Stellar and interstellar FUV entering the disk along sight lines to the central star and at high angle, respectively, are shown schematically. Dashed lines refer to the optically thin FUV wavelengths that dissociate $C^{18}O$ and $C^{17}O$. In the process considered here, H_2O enriched in ^{18}O and ^{17}O is formed near $n(H_{tot})$ ~ 10^6 contours as a product of CO photodestruction. The isotopically heavy water is then transported by turbulent forces to the inner disk (grey arrows). B: Closeup of one quadrant of the disk showing contours for the rate of CO dissociation (solid black) assuming solar C/H and O/H. Grey lines mark CO optical depths (τ_{CO}) of 1 (upper) and 4 (lower). The region between $\tau_{CO}=1$ and $\tau_{CO}=4$ shown in grey is where self shielding of stellar FUV by CO is pronounced (the different locations for the CO, $C^{17}O$ and $C^{18}O$ $\tau=1$ surfaces are not resolved at this scale, see Fig. 3).

By assuming a solar-like ratio of CO to H_2 in the gas phase (e.g., gas in an accretion disk or in a molecular cloud in the interstellar medium), one can use the FUV shielding functions for CO (Lyons and Young, 2005a; van Dishoeck and Black, 1988) to show that oxygen isotope fractionation by CO photodissociation is expected in regions where the total column density of hydrogen, N_H, is $\sim 10^{19}$ to 10^{22} cm^{-2} (Fig. 1). One can also use typical relationships between N_H and extinction of visible light, or Av expressed in magnitudes ($\Delta m = mag = 2.5 \log(I_2/I_1)$ where I_2 and I_1 are two different intensities of light), by $\sim$ 0.1 micron-sized dust grains (Lee et al., 1996) to show that oxygen isotope fractionation by CO photodestruction is expected where Av ranges from $\sim 5\times10^{-3}$ to 5. Larger sized dust grains such as might be found in a disk reduce the Av corresponding to regions where CO self shielding is expected by approximately 10 fold. These ranges in N_H and Av serve as general guides for assessing the likely locations for CO isotope-selective photodissociation.

3. The pivotal role of H_2O

Solar abundances of the elements and the kinetics of gas phase reactions indicate that approximately half of the total oxygen in a protoplanetary disk resides as CO. Another 1/3 is contained in H_2O with the remainder as lithophile oxides (Anders and Grevesse, 1989; Fegley, 2000). Evidently, water played a central role as the carrier of ^{16}O-depleted oxygen in the early Solar System. Clayton and Mayeda (1984) recognized the importance of H_2O as a reservoir for ^{16}O-depleted oxygen in the solar nebula based on the isotopic composition of secondary minerals in chondrites. Yurimoto and Kuramoto (2002, 2004) pointed out that there should have been a reciprocity in $\Delta^{17}O$ between H_2O and CO in the protosolar molecular cloud. Lyons and Young (Lyons and Young, 2005b; Young and Lyons, 2003) showed that the same isotopic reciprocity likely existed between H_2O and CO in cold portions of the protosolar accretion disk high above the midplane.

Water is a likely driver for the oxygen isotopic evolution of the Solar System because H_2O forms readily from O liberated by CO photodissociation, and because H_2O gas exchanges oxygen isotopes with silicate rapidly while CO does not. Yu et al. (1995) showed that 50% oxygen isotope exchange occurs between molten silicate and H_2+H_2O gas at 1773 K and 1 bar after 5 min. These authors argued that at nebular pressures ($\sim 10^{-5}$ to 10^{-8} bar) 50% exchange would take 10 h; exchange of oxygen between molten silicate and H_2O gas is efficient. Conversely, analogous experiments involving CO and silicate show no evidence of isotopic exchange under similar conditions (Bosenberg et al., 2005).

The pivotal role of H_2O in the isotopic evolution of the solar nebula is suggested by numerous studies showing that $\Delta^{17}O$ of water during chondrite formation was substantially greater than that of rock (Choi et al., 1998; Clayton and Mayeda, 1984; Young et al., 1999). Meteoritic studies suggest that the inner solar nebula became enriched in $^{17,18}O$ with time (e.g., Choi et al., 1998; Wasson et al., 2004) and there is plentiful evidence for oxygen isotopic exchange between surrounding nebular gas and meteoritic constituents, including calcium–aluminum-rich inclusions (CAIs) (Fagan et al., 2004; Yoshitake et al., 2005; Yurimoto et al., 1998) and chondrules (Maruyama et al., 1999; Wasson et al., 2004). These observations appear consistent with the scenario of gradual H_2O enrichment in the inner disk during disk evolution.

Most recently, Sakamoto et al. (2007) found what appear to be aqueous alteration products in a carbonaceous chondrite suggesting water $\delta^{18}O$ and $\delta^{17}O$ values as high as 180‰ relative to SMOW. These high values were evidently preserved in these first wisps of aqueous alteration because the degree of water–rock exchange of oxygen isotopes was limited (Young, 2007). These data constitute our best estimate of the water oxygen isotope ratios in the inner Solar System prior to exchange with rock.

The amount of water that exchanged oxygen with rock in the inner Solar System can be estimated using these new initial water $\delta^{18}O$ and $\delta^{17}O$ values. For this purpose we use the oxygen mass-balance expression $\delta^{f}_{water}-\delta^{0}_{water}=F\,(\delta^{0}_{rocks}-\delta^{f}_{rocks})$, where F is the number of oxygens in rock divided by the number of oxygens in water (the rock/water ratio in oxygen units) and the superscripts 0 and f refer to initial and final isotope ratios of water and rock in per mil. Gas is assumed to be entirely water because we need only consider the gas that readily exchanges oxygen isotopes with silicate. If the final and initial $\delta^{18}O$ (and $\delta^{17}O$) values for early Solar System rock were 0 and − 50‰, respectively, as suggested by data for CAIs and rocky planets, and the values for H_2O were 0 and + 180‰, respectively, as suggested by the latest estimates for Solar System water, then $F=3.6$. For comparison, solar abundances of O, C, Si and Mg (Anders and Grevesse, 1989; Melendez, 2004; Prieto et al., 2002) yield a solar value for F of $\sim$ 0.34 (obtained by solving for number densities of H_2O, CO, SiO_2, and MgO in terms of those for solar O, C, Si, and Mg). The implication is that an enhancement in the silicate dust/water ratio of approximately 10 fold occurred in regions in the solar

protoplanetary disk where gas and silicate oxygen isotopes exchanged. Conversely, the solar value for F would imply an initial $\delta^{18}O$ for Solar System water of only 19.5‰.

4. Model for CO self shielding in the solar circumstellar disk

Within the circumstellar disk that was the solar nebula, the surfaces of the disk were prime locations for creating and preserving the isotopic effects of CO self shielding (Fig. 1). In this work reaction network calculations were carried out along the surfaces of a model disk where H_2 number densities are on the order of $\sim 10^5$ to 10^6 cm^{-3} (pressure $\sim 10^{-14}$ bar) and where CO photodissociation occurs. The goal was to characterize the chemical and isotopic effects of photolysis in these photoactive regions. A model circumstellar disk provided estimates of gas column densities along sight lines to the central star. These column densities control the rates of photolysis in the photoactive layers of the disk. Results provide estimates of rates of reactions and degrees of isotope fractionation as a function of position in the disk in those places where CO self shielding should have occurred. A box model was then used to examine how the isotopic signals acquired in the surface regions of the disk could have been dispersed to the region of terrestrial planet formation.

The first quantitative model for the oxygen isotopic consequences of CO self shielding in the solar circumstellar disk was given by Lyons and Young (2005a). These authors present a one-dimensional calculation at one distance from the star in which a UV flux perpendicular to the surfaces of the disk caused liberation of ^{16}O-depleted O by CO photodissociation. The code included 375 reactions among 96 species and gas-grain reactions that permitted H_2O to form on grain surfaces from the liberated O. Vertical mixing from the disk "photosphere" (the photoactive horizons) to the midplane was included by approximating a turbulent eddy diffusion coefficient with the turbulent viscosity $\nu_t = \alpha\, cH$ where c is the sound speed, H is the vertical scale height and α is the parameter that prescribes the strength of turbulent mixing. The present study differs from that earlier work by 1) invoking a larger reaction network at the expense of ignoring mixing explicitly in the chemical calculations; 2) considering UV illumination from the central star; 3) investigating rates of reaction as a function of radial position in the disk; and 4) considering advective transport from regions of active photochemistry to denser portions of the inner disk where rock formation occurs.

4.1. Reaction network

More than 500 species and 7600 reactions are used in the new reaction network employed here. The code utilizes a modification of the University of Manchester Institute of Technology database for astrochemistry (UMIST, rate99) (Le Teuff et al., 2000). The kinetic reaction network was constructed by adding singly-substituted oxygen isotopologues for each O-bearing species in the rate99 database (i.e., addition of $M^{17}O$ and $M^{18}O$ for each $M^{16}O$). Rates of reactions were obtained by convolving the rate constants in the revised kinetic database with a simple model for number densities, temperatures, and FUV flux as a function of circumstellar radial distance R and height above the midplane Z in a disk (Fig. 1, Section 4.2, (Aikawa and Herbst, 2001)). Use of a modification of the UMIST rate99 database is justified in so far as conditions that pertain to outer regions of disks, the regions of interest here, are similar to ISM conditions (with the exception of the ultraviolet field, see below). A complete listing of the new kinetic database, isotope99v4. rates, can be found in the Online supplementary material. For this work the phosphorous-bearing species were excluded.

Rate constants for the resulting reactions for the O isotopologues were adjusted to allow for mass-dependent isotope fractionation using reduced masses for collisions between reactants applied to the preexponential terms. For example:

$$\begin{aligned} &H + H_2{}^{16}O \rightarrow {}^{16}OH + H_2 \\ &\qquad k_f = 1.5900 \times 10^{-11}\ \exp(-E_a/(kT)) \end{aligned} \tag{1}$$

$$\begin{aligned} &H + H_2{}^{18}O \rightarrow {}^{18}OH + H_2 \\ &\qquad k'_f = 1.5858 \times 10^{-11}\ \exp(-E_a/(kT)). \end{aligned} \tag{2}$$

where k_f and k'_f (cm^3/s) are the forward rate constants for the indicated isotopologues of H_2O, E_a is the activation energy for the reaction, and k is Boltzmann's constant. Isotopologue branching ratios, as in $QOH + O_2H \rightarrow H_2O_2 + QO$ vs. $QOH + O_2H \rightarrow H_2QO + O_2$, where Q represents ^{18}O or ^{17}O and O represents ^{16}O, were taken to be 1/2. Isotopic effects of bond rupture, including zero-point energy differences and isotope effects of mass-dependent vibrational frequencies along the reaction coordinate, are important contributors to mass fractionation at low temperatures but are excluded here because the data necessary to evaluate these effects are lacking for most reactions. Nevertheless, we can evaluate the general magnitude of these effects in the context of transition state theory. The isotope

fractionation factor α_{iso} associated with forward progress of a reaction will be

$$\alpha_{iso} = \frac{\nu'_{col}}{\nu_{col}} \frac{\nu*'}{\nu*} \exp((\Delta ZPE - \Delta ZPE*)/(kT)) \quad (3)$$

where ν_{col} and ν'_{col} are the collision frequencies among reactants for the abundant and rare isotopologues, respectively (e.g., the preexponential terms in reactions (1) and (2)), $\nu*$ and $\nu*'$ are the vibrational frequencies for the reaction coordinate of the two isotope-specific transition states, ΔZPE is the zero-point energy difference between the rare and abundant isotopologues of reactants (ZPE′–ZPE) and ΔZPE* is the analogous difference in zero-point energies for the transition state isotopic species. In general one expects the reactant zero-point energy terms to dominate over the transition state terms (bonds in the latter being weaker). Where estimates of the relevant zero-point energies and reaction coordinate mode of vibration can be evaluated, it appears that the contributions of these terms to α_{iso} can be at least as large, and in many cases considerably larger than, collisional frequency contributions. For example, oxygen isotope ΔZPE–ΔZPE* are on the order of 1 to 10 K (e.g., Langer et al., 1984), corresponding to mass-dependent shifts in δ values of 20 to 180‰ at 50 K. For reaction (1) the transition state has been investigated (Yang et al., 2001), confirming that the reactant zero-point energy terms dominate, but for most reactions used here the transition states have not been investigated. Future work will explore the influence of $\nu*$ and $\nu*'$ as well as ΔZPE and ΔZPE* on mass-dependent oxygen isotope fractionation in disk settings using a parsimonious reaction set.

Several oxygen isotope exchange reactions were added to the reaction network. Simple isotopic exchange between O and CO is notoriously sluggish. For example, the rate constant for Q+CO=O+CQ varies from 6×10^{-36} to 9×10^{-14} cm^3 s^{-1} at 60 K to 500 K, respectively (Jaffe and Klein, 1966). At the higher temperature this rate constant is comparable to other exchange reactions, including that for OH+CQ=QH+CO, but at these temperatures the concentration of O is too low for the reaction to be relevant. For this reason we include oxygen isotope exchange explicitly between OH and H_2O (Dubey et al., 1997), OH and CO (Greenblatt and Howard, 1989), and HCO^+ and CO (Langer et al., 1984) but not O and CO.

Gas–dust grain reactions were also added to the reaction network. The adsorption/desorption reactions, involving H, H_2, CO, O, OH, and H_2O and their isotopologues are listed at the end of Table 1 of the Online supplemental material. Freeze out rate constants are of the form $k_{ads} = \langle \pi r_g^2 \rangle \hat{v}\, n_g$ s^{-1} where r_g is the radius of dust grains, $\hat{v} = \sqrt{8kT/(\pi m)}$ is the mean gas velocity, m is the atomic or molecular mass of the gas species, and n_g is the dust grain number density, assumed to be 10^{-12} relative to n(H) in these calculations (results reported here are not particularly sensitive to the value for n_g within several orders of magnitude). Rate constants for thermal desorption have the form $k_{des}=\nu \exp(-E_b/(kT))$ s^{-1} where E_b is the binding energy. Values for E_b for adsorbed H, H_2, CO, O, OH, and H_2O (H_{ads}, $H_{2,ads}$, CO_{ads}, O_{ads}, OH_{ads}, and H_2O_{ads}) are taken from the literature (Hasegawa et al., 1992; Willacy et al., 1998) assuming an adsorption bond frequency of 10^{12} s^{-1}.

We are particularly concerned with the formation of water ice and so intragrain surface reactions involving H_{ads} and O_{ads} to produce OH_{ads}, $H_{2,ads}$, and H_2O_{ads} are included. Although part of the reaction network, the reaction $O_{ads}+H_{2,ads}\rightarrow H_2O_{ads}$ has a substantial activation barrier (E_a/k=2100 K), making it an ineffective means for forming water on grain surfaces (Caselli et al., 1998). A faster path to H_2O_{ads} production, and the one dominant in the present calculations, is $H_{ads}+O_{ads}\rightarrow OH_{ads}$ followed by $H_{ads}+OH_{ads}\rightarrow H_2O_{ads}$ (Hasegawa et al., 1992).

For each of the species M the reactions include two-body formation with rate constant k_f (cm^3 s^{-1}, including intragrain surface reactions among adsorbed species): A+B→M+N; photolysis with rate constant β (s^{-1}): M+hν→W+Q; cosmic ray ionization with rate ζ_{crp} (s^{-1}): M+p→M$^+$+e+p; photoionization with rate constant $\zeta_{X\text{-}ray}$: M+hν→M$^+$+e; and two-body destruction with rate constant k_d (cm^3 s^{-1}): M+X→Y+Z. To these we add the adsorption/desorption reactions with rate constants described above. The time-dependent evolution of 546 species M in terms of progress of 7603 reactions in this study is then obtained by solving the coupled ordinary differential equations of the form:

$$\frac{dn(M)}{dt} = k_f n(A) n(B) + k_{des} n(M_{ads}) - n(M) \times (\beta_M + \zeta_M + k_d n(X) + k_{ads}) \quad (4)$$

where $\zeta_M=\zeta_{X\text{-}ray}+\zeta_{crp}$ and $n(i)$ are number densities for species i. In this work I have parameterized the X-ray enhancement of ionization in the disk relative to the interstellar medium (built into the rate99 database) by fitting ζ_M as a function of visual extinction as presented in Table 1 of Aikawa and Herbst (1999). For reference, the typical n_e/n_H (electron number density

relative to total hydrogen) for the CO photochemically active layer of the disk 20 AU from the central star in the present calculations is on the order of 10^{-5} to 10^{-4}.

The calculations account for CO and H_2 mutual, self, and molecular shielding using previously published shielding functions (Lee et al., 1996; Lyons and Young, 2005a) and broad-band absorption of FUV by H_2O with a cross section of 2×10^{-17} cm^2 for $\lambda=90$ to 110 nm. Isotope specificity of absorption by H_2O can be ignored at these shorter wavelengths (Liang et al., 2004; Miller and Yung, 2000). The rate constants for CO photodissociation are modified accordingly with expressions of the form (using photodissociation of $C^{16}O$ as the example)

$$\beta_{C^{16}O} = \beta^{o}_{C^{16}O}\exp(-\sigma_{C^{16}O,C^{16}O}N_{C^{16}O})\exp(-\sigma_{C^{16}O,C^{18}O}N_{C^{18}O})\exp(-\sigma_{C^{16}O,C^{17}O}N_{C^{17}O})\exp(-\sigma_{C^{16}O,H_2}N_{H_2})\exp(-\sigma_{C^{16}O,H_2O}N_{H_2O})\exp(-\gamma_{C^{16}O}Av) \quad (5)$$

where $\beta^{o}_{C^{16}O}$ is the unshielded photolysis rate constant for $C^{16}O$ (in this example), $\sigma_{C^{16}O,j}$ is the absorption coefficient for species j over the wavelengths corresponding to $C^{16}O$ photodissociation, N_j is the column density for species j, and $\gamma_{C^{16}O}$ is a factor that converts the visual extinction Av to the appropriate UV wavelengths. The values for β^{o} are dependent on the column densities at any given position in the disk. These column densities come from the disk model described in Section 4.2. Equations analogous to Eq. (5) modify β^{o} values for $C^{17}O$ and $C^{18}O$. In practice the shielding functions $\Theta_i = \sum_j \exp(-\sigma_{i,j}N_j)$ in Eq. (5) are further modified for the differing molecular shielding effects of H_2 on $C^{17}O$ and $C^{18}O$ as described by Lyons and Young (2005a).

The set of stiff ordinary differential equations comprising the reaction network are solved using Gear's method as implemented by the Lawrence Livermore National Laboratory Solver for Ordinary Differential Equations (DLSODE, Fortran 77). A series of scripts for analyzing the results of the calculations has also been developed.

In all of the calculations presented here the solar oxygen isotope ratios were used as initial oxygen isotopologue ratios (within the range of ISM values, the choice of initial ratios makes little or no difference to the final results). Incorporation of oxygen isotopologues into the database provides a convenient check on accuracy of the reaction network calculations. Mass independent oxygen isotope partitioning can occur in the code only by CO photodissociation. By turning off the UV flux in the calculations we should obtain mass-dependent isotope fractionation only, affording an accuracy check analogous to the tests performed in the laboratory whereby deviations from mass-dependent fractionation are usually indicative of analytical error (e.g., mass interferences in mass spectrometry). This test was applied to the models in this study. The tests show that accurate calculations obtain for species spanning 10 orders of magnitude in number density. Beyond this range numerical inaccuracies creep in to produce spurious deviations from mass dependent isotope fractionation.

4.2. Disk model

The disk model used here is that described by Aikawa and Herbst (1999, 2001). It is the so-called Kyoto model, and depicts a static disk of mass comparable to the minimum mass gaseous solar nebula. A simple static model for the disk such as this permits computing power to be focussed on solving the reaction network equations at critical positions in the disk while still providing reasonable approximations to the UV radiation field and column densities of CO and H_2.

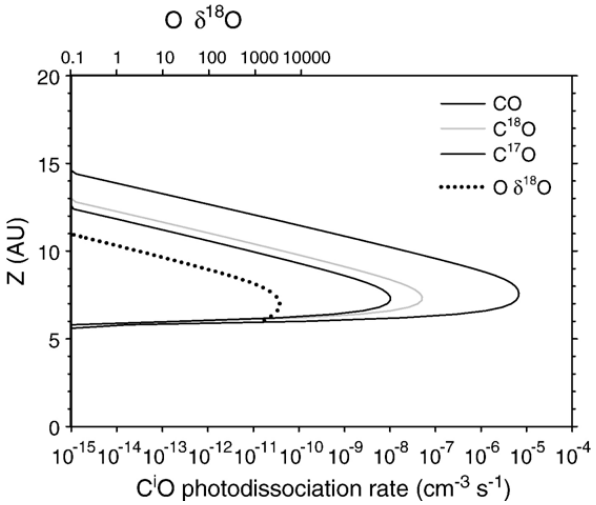

Fig. 2. Calculated CO photodissociation rates as a function of height above the midplane Z (AU) for the model circumstellar disk at a heliocentric radius R of 20 AU. A constant $n(CO)/n(H)$ of 2.45×10^{-4} was used to construct the contours (see text), meaning that the rates shown here comprise the initial condition for progress of photochemistry. C^iO column densities (where i is 16, 17 or 18) required for calculating FUV shielding functions were obtained by integration along sight lines toward the central star corresponding to $Z=\tan\theta\ R$ where θ is the angle between the sight line and the midplane of the disk. The figure illustrates the differences in photolysis rates for the three oxygen isotopologues of CO considered. Also shown (dashed line) are the oxygen isotopic ratios for atomic oxygen liberated by CO photolysis implied by the Z-dependent ratio of the rates of C^iO photodissociation. These rate ratios are initial conditions and will change as photolysis progresses and abundances of CO isotopologues evolve.

Mixing of gas and dust is addressed using the box model approach described in Section 4.3. Isotope-specific rates of CO photodissociation obtained by combining the kinetic reaction network described above with the static disk model are shown in Fig. 2. The rates shown in Fig. 2 are the initial condition for the model. Actual isotope effects in gas species in the disk are diluted by mixing, as described in Section 4.3.

The spatial distribution of mass in the disk is prescribed by an equation for total hydrogen number density $n(\mathrm{H_{tot}})$ in terms of radial distance from the central star, R, and height above the midplane, Z. The expression relating $n(\mathrm{H_{tot}})$ to R and Z is

$$n(\mathrm{H_{tot}}) = 1.9x10^{9}\left(\frac{R}{100\mathrm{AU}}\right)^{-11/4}\exp\left(\frac{-GM_{\odot}\hat{m}}{R\ kT}\right)$$
$$\exp\left(\frac{-GM_{\odot}\hat{m}}{(R^2+Z^2)^{1/2}\ kT}\right) \quad (6)$$

where G is the gravitational constant, $M_{\odot}$is the mass of the central star, chosen to be one solar mass, $\hat{m}$ is the mean mass of gas molecules (i.e., H_2>He, so that $\hat{m}=2.37\times1.66\times10^{-27}$ kg), and temperature $T=28$ (R/100 AU)$^{-1/2}$. Temperature is assumed to vary with R but not Z in this simple model. As an initial condition we assume $n(\mathrm{CO})/n(\mathrm{H})=2.45\times10^{-4}$ throughout the disk with initial $n(\mathrm{H_2O})$ calculated from the O not in CO. These values are consistent with solar abundances of C, O, and H (Anders and Grevesse, 1989; Melendez, 2004; Prieto et al., 2002). Initial concentrations of minor elements (N, Si, etc.) were obtained from their solar abundances.

Eq. (6) results in a flared disk geometry (Fig. 1) that is consistent with observations of many circumstellar accretion disks (Kenyon and Hartmann, 1987). There are two sources of FUV at the surfaces of a circumstellar disk (Fig. 1). One is ambient UV from the surrounding environs entering the disk at a high incident angle. The other is from the central star itself where light travels on lines of sight from the star through the disk. In the former case column densities for Eq. (5) at a position R and Z in the disk are obtained by integration of number densities along the Z direction towards the midplane. In the latter case column densities are obtained by integration along sight lines toward the central star corresponding to $Z=\tan\theta\ R$ where θ is the angle between the sight line and the midplane of the disk (Fig. 2). A disk with concave upper surfaces (relative to the midplane) such as that used here intercepts more light along a sight line to the central star than a non-flaring disk. This effect increases with distance from the central star (Kenyon and Hartmann, 1987) and maximizes the potential for photochemistry within the optically thin surfaces.

The FUV flux at $R=100$ AU was chosen to be 200× local ISM (i.e., 200 Habing where 1 Habing corresponds to $\sim 3\times10^{-8}$ photons cm^{-2} s^{-1} Hz^{-1} at 90 to 105 nm, (Jura, 1974)) in the calculations presented here. This value is a minimum suggested by observations of T-Tauri stars (Bergin et al., 2004). Calculations reported here (except where noted) are based on illumination from the central star so that the FUV flux increases according to a scale factor $\chi=200\times(100\mathrm{AU}/R)^2$. Under these conditions UV from the central star dominates the photochemistry of most of the disk. Photochemical rate constants in the reaction network are multiplied by χ because the database refers to normal ISM fluxes. Visual extinction was modelled as $\mathrm{Av}=2.34\times10^{-23}\ N(\mathrm{H})$ (Kamp and Bertoldi, 2000). This extinction model assumes a uniform dust grain size of 3 μm. It represents an attempt to account for grain coarsening in disks relative to the interstellar medium. The 3 μm grain size may well be an over estimate, making the adopted Av values minima for these calculations. Typical values for Av in the photochemically active layers of the disk are on the order of 10^{-4} with this model. Values for γ were taken from the UMIST database. Larger values for γAv were adopted in the disk chemistry models of Willacy and Langer (2000).

No attempt was made to iterate between the reaction network calculations and the column densities provided by the static disk model. This necessary simplification will have some affect on the accuracy of the results, although the inaccuracy will be mitigated by the flared disk geometry. The code accounts for photon absorption and emission by reactions but does not simulate radiative transfer for the disk as a whole. This simplification is justified since we are not concerned here with modelling spectroscopic observations of disks but rather with tracking the chemistry at a given position within the disk. In the treatment that follows, no explicit adjustments of gas temperatures due to ionization by X-rays (e.g., Glassgold et al., 2005) have been made. More work is needed in this area, but column-density considerations suggest that self shielding by CO should occur deeper in disks than dramatic X-ray ionization heating (Glassgold et al., 2005), suggesting that the thermal effects of X-rays from the central star may be confined to layers above those of concern here.

4.3. Disk box model (transport)

Transport within the disk is simulated in this work using a 4-box model. The four reservoirs comprising the model are: (1) the star; (2) the optically thin surfaces of the

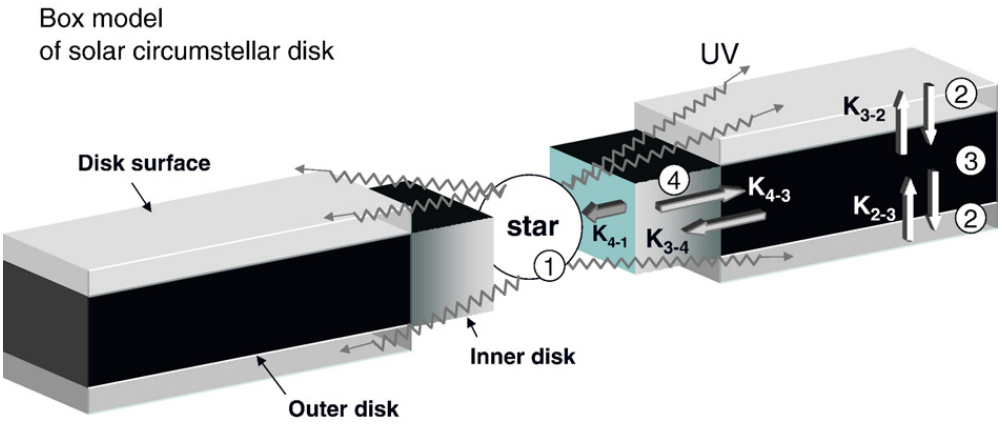

Fig. 3. Schematic showing a box model for the evolution of oxygen isotope ratios in the early Solar System. Numbers refer to boxes representing reservoirs in the circumstellar disk and star system. These reservoirs are: (1) star; (2) photoactive layers of the disk; (3) outer disk; (4) inner disk where terrestrial planets form. The k_{ij} are rate constants for transport while k_{photo} is the rate constant for conversion of CO to H_2O at the disk surfaces (in reservoir (2)).

disk high above the midplane (i.e., the photoactive layer); (3) the outer portions of the disk near the midplane (e.g., within one scale height of the midplane beyond the asteroid belt); and (4) the inner disk that will give rise to the asteroid belt and terrestrial planets (Fig. 3). In this model, transfer of mass between reservoirs is simulated using a first-order rate equation, a technique used with success in modelling geochemical cycles (Lasaga, 1980). Given a number density or mass of species i in each reservoir j, n_{ij}, the transfer of material can be written with a system of four ordinary differential equations.

As an example, consider the equations for the time-dependent number density of an oxygen isotopologue i of CO that is subject to photodestruction in the outer surfaces of the disk. The mass balance equations representing the time-dependent evolution of the amount of C^iO in each of the four reservoirs comprising the model accretion disk are then

$$\frac{\mathrm{d}n_{i1}}{\mathrm{d}t} = k_{41}n_{i4} - k_{14}n_{i1}$$

$$\frac{\mathrm{d}n_{i2}}{\mathrm{d}t} = k_{32}n_{i3} - (k_{23} + k_{\mathrm{photo},i})n_{i2}$$

$$\frac{\mathrm{d}n_{i3}}{\mathrm{d}t} = k_{43}n_{i4} + k_{23}n_{i2} - (k_{32} + k_{34})n_{i3}$$

$$\frac{\mathrm{d}n_{i4}}{\mathrm{d}t} = k_{34}n_{i3} + k_{14}n_{i1} - (k_{43} + k_{41})n_{i4} \qquad (7)$$

where n_{ij} is the amount of C^iO in reservoir j, k_{jk} refers to the first-order rate constant (s^{-1}) for transport of C^iO from reservoir j to reservoir k and $k_{\mathrm{photo},i}$ is the effective photodissociation rate constant for C^iO. In constructing Eq. (7) we ignore short-circuit pathways such as transfer from the inner edge of the disk to the outer distal surfaces as might occur in an x-wind (Shu et al., 1996) (in other words here $k_{42}=0$), although the principles used to construct the equations allow for such a process if desired. For purposes of illustration one can simplify Eq. (7) further by assuming that convective forces in the disk and mass accretion onto the disk maintain a constant concentration of CO in the surface layer. In other words we assume for illustration purposes that the disk surfaces reach a balance between UV photodestruction of CO and retreat of the surfaces deeper into the disk. In such a case $\mathrm{d}n_{i2}=0$ and the equations in matrix form become

$$\begin{pmatrix} \frac{\mathrm{d}n_{i1}}{\mathrm{d}t} \\ \frac{\mathrm{d}n_{i3}}{\mathrm{d}t} \\ \frac{\mathrm{d}n_{i4}}{\mathrm{d}t} \end{pmatrix} = \begin{pmatrix} -k_{14} & 0 & k_{41} \\ 0 & -k_{34} & k_{43} \\ k_{14} & k_{34} & -(k_{43}+k_{41}) \end{pmatrix} \begin{pmatrix} n_{i1} \\ n_{i3} \\ n_{i4} \end{pmatrix} + \begin{pmatrix} 0 \\ -k_{\mathrm{photo},i}n^{o}_{i2} \\ 0 \end{pmatrix} \qquad (8)$$

where n^{o}_{i2} is the initial value for n_{i2}. We can rewrite Eq. (8) more compactly as

$$\dot{\mathbf{n}}(t) = \mathbf{A}\mathbf{n} + \mathbf{b}. \qquad (9)$$

Eq. (9) represents the system of equations for the time-dependent evolution of abundances of species i in different parts of the accretion disk in terms of rates of transport across the disk. The solution to Eq. (9) and systems analogous to it is in general (Lasaga, 1980)

$$\dot{\mathbf{n}}(t) = \sum_{l=1}^{n} c_l \boldsymbol{\Psi}_l \exp(\lambda_l t) + \mathbf{X}\int \mathbf{X}^{-1}\mathbf{b}\,\mathrm{d}t \qquad (10)$$

where n is the dimension of coefficient matrix $\mathbf{A}$ (3 in our case), c_l is a scalar integration constant determined by the initial values n_{ij} (n^{o}_{ij}), $\boldsymbol{\Psi}_l$ is the lth eigenvector of

A, λ_l is the lth eigenvalue of **A**, **X** is the $n \times n$ matrix composed of n vectors $\mathbf{\Psi}_l \exp(\lambda_l t)$, $\mathbf{X}^{-1}$ is the inverse of **X** and **b** is the forcing function in Eq. (8). Values for c_l can be obtained from $\mathbf{c}=\mathbf{E}^{-1}\,\mathbf{n}^{\circ}$ where **E** is the matrix of eigenvectors, **c** is the vector of constants sought, and $\mathbf{n}^{\circ}$ is the vector of n_{ij}° values. Lasaga (1980) showed that there will be $n-1$ non-zero eigenvalues for Eq. (10). In the present example the two non-zero eigenvalues are $\lambda_1 = -k_{34}$ and $\lambda_2 = -k_{41}$. The response time for changes in $n_C i_O$ in the various reservoirs in our simple model is therefore the larger of $1/k_{34}$ or $1/k_{41}$.

Eq. (10), as one example of a box model for a protoplanetary disk, is simple enough to be evaluated analytically. The result provides an appreciation for the factors that control the number densities of a species in a dynamically active disk setting. Expansion of Eq. (10) for our example gives for n_i in the inner disk (reservoir 4)

$$n_{i4}(t) = \left(\frac{k_{34}}{k_{34}-k_{41}} n_{i3}^{o} + n_{i4}^{o}\right)\exp(-k_{41}t) - \frac{k_{34}}{k_{34}-k_{41}} n_{i3}^{o}\exp(-k_{34}t) - k_{\mathrm{photo},i} n_{i2}^{o}\left(\frac{1-\exp(-k_{34}t)}{k_{41}-k_{34}} + \frac{k_{34}}{k_{41}}\frac{(1-\exp(-k_{41}t))}{(k_{34}-k_{41})}\right). \quad (11)$$

From Eq. (11) the steady-state solution for $n_{i4}(t)$ is

$$\lim_{t\to\infty} n_{i4}(t) = k_{\mathrm{photo},i} n_{i2}^{\circ}\left(\frac{k_{34}-k_{41}-1}{k_{41}-k_{34}}\right) \quad (12)$$

showing that the steady-state amount of C^iO in the inner disk is determined by the rate of photodissociation in the surface layers, the radial flow of CO from the outer to the inner disk, and the rate of CO accretion to the star if the abundance of CO is in steady state in the photoactive layers.

Eqs. (11) and (12) are examples showing how box models can be used to track the time-dependent evolution of molecular species in a dynamic circumstellar disk. In the present study equations analogous to Eq. (7) were solved numerically for the time-dependent abundances of $H_2^{16}O$, $H_2^{17}O$, and $H_2^{18}O$ together with $C^{16}O$, $C^{17}O$, and $C^{18}O$ in each of the four reservoirs shown in Fig. 3. The solutions are analogous to Eq. (11) but without the restrictions that enabled us to obtain the analytical result presented above.

5. Model results

5.1. Rates of CO photodissociation

Oxygen isotope-specific photodissociation of CO occurs at total gas column densities of 10^{19} to 10^{22} cm^{-2} when CO/H_2 is approximately 10^{-4} (i.e., for solar C/O). As a result, liberation of ^{18}O and ^{17}O enriched O from CO will be focussed along surfaces in the disk were $Z \sim 1/4$ to $1/3$ R with either high incident angle of illumination (not shown) or along sight lines from the central star (Fig. 1). The isotope effect is maximized where the optical depth τ ($\tau=\sigma N$) for CO is ~ 4.

Rates of CO photodissociation with a uniform vertical FUV flux and rates due to FUV illumination along stellar sight lines toward the central star (with the same flux at 100 AU) are similar at large radial distances R from the star (e.g., $R \geq 100$ AU). Differences become substantial, however, as the FUV flux rises sharply (as $1/R^2$) in the latter case with proximity to the star (Fig. 1). In this work focus is placed on $R<100$ AU where illumination from the central star dominates. The calculations presented below show that FUV fluxes at $R<5$ AU are so great and the attending rates of CO photodissociation so rapid that sequestration of oxygen isotope signals of CO self shielding in the oxygen species that remain is effectively precluded.

5.2. Spatial variations in the oxygen isotope effects of CO photodissociation

At $R>10$ AU the net result of CO photodissociation is wholesale conversion of CO gas to H_2O ice in the photoactive layers of the disk (Fig. 4). Yurimoto and Kuramoto (2004) suggested that H_2O formation is mediated primarily on dust grain surfaces. The present results show that ice forms on grains largely by freezing H_2O gas formed through the H_3^+ channel (Herbst, 2000)

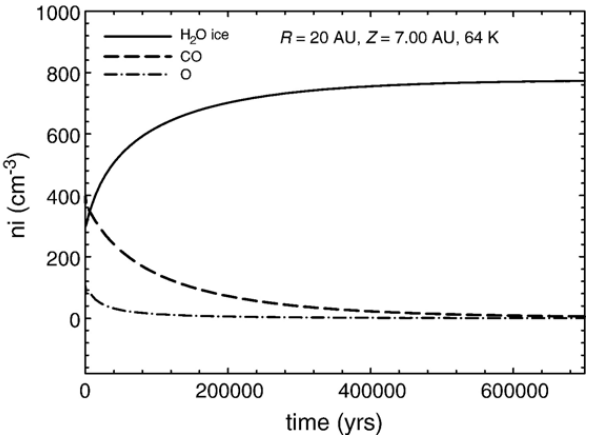

Fig. 4. Calculated time evolution of number densities of CO, H_2O ice, and O at $R=20$ AU and $Z=7.00$ AU in the circumstellar disk. The calculation refers to a static disk (i.e., no mixing) and illustrates the timescale for conversion of CO to H_2O. Note that the e-fold time for loss of CO to produce H_2O is $\sim 1\times10^5$ yr.

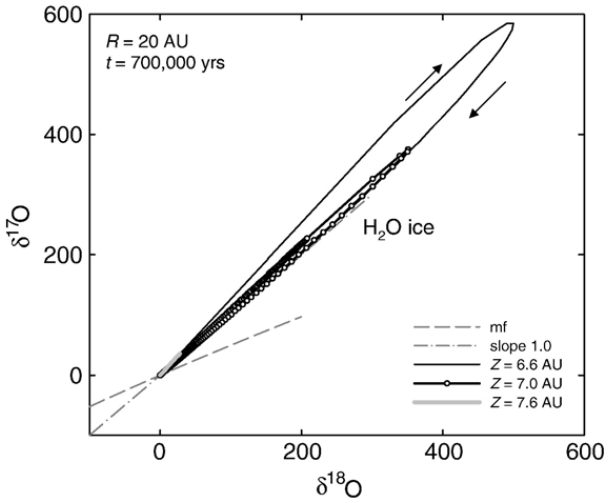

Fig. 5. Calculated time evolution of $\delta^{17}O$ and $\delta^{18}O$ in water ice at $R=20$ AU and $Z=7.6$, 7.0 and 6.6 AU in a static circumstellar disk. The δ values are relative to the initial composition of the system. Increments of time are shown for the $Z=7.0$ altitude by open dots; closely spaced open dots at the start of the curve represent 70 yr intervals while the more widely spaced dots refer to 7 kyr intervals. All curves end at 700,000 yr. Arrows mark the direction of time for the curves. The plot shows that the isotope effects of CO self shielding are greatest lower in the disk as the optical depth of $C^{16}O$ approaches ~ 4. The full isotope effect in the photoactive layer is the integral of δ with respect to Z. Also shown are the mass fractionation line through the initial oxygen isotopic composition (mf) and a slope − 1.0 line through the initial composition.

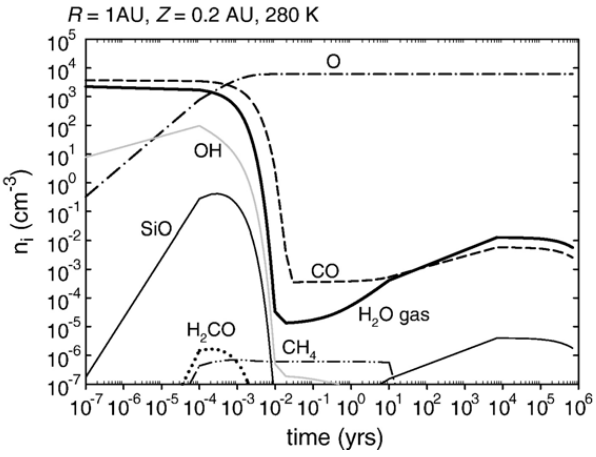

Fig. 6. Time evolution of number densities of CO, H_2O ice, O, H_2CO, SiO, and CH_4 at $R=1.0$ AU and $Z=0.2$ AU in the model static circumstellar disk. Note the rapid timescale of evolution at these number densities and FUV fluxes compared with reactions at $R=20$ AU. A steady state is achieved with respect to H_2O abundance in approximately 10^3 to 10^4 yr. Rapid loss of CO makes O and H_2O the dominant oxygen reservoirs in this part of the disk if the system remains closed to CO addition from outside.

(initiated by reaction 1382 in the reaction network, Table 1 of the Online supplementary material). The timescale for H_2O ice formation from CO is on the order of 10^5 yr (Fig. 4).

At $R>5$ AU H_2O ice produced by CO photodissociation forms along a slope-1 line in $\delta^{17}O$ vs. $\delta^{18}O$ space (Fig. 5). This is true even in the presence of the pre-exponential mass-dependent fractionations used in these calculations. At $R \sim 10$ AU in the model a steady state is achieved at disk surfaces such that reactions that produce CO are balanced by the conversion of CO to H_2O ice. Here the loops in Fig. 5 become curves that terminate at a point with steady-state $\delta^{17}O$ and $\delta^{18}O$ values that are on a line with a slope of ~ 1 in three-isotope space. This steady-state contrasts with the behaviour shown in Fig. 5 in which product H_2O rises along the slope-l line and then, eventually, returns to the original oxygen isotope ratios once CO is largely burned away.

At $R \leq 5$ AU reaction timescales are too rapid to preserve the isotopic effects of CO photodissociation due to the high FUV flux (Figs. 6 and 7). As a result, non-mass dependent oxygen isotope fractionation due to CO photolysis is necessarily an outer disk phenomenon because there FUV fluxes are low enough to permit trapping of the CO isotope effect in water. Self shielding by CO cannot be an explanation for $\Delta^{17}O$ variability in the solar system if it occurred near to the star at $R \leq 5$ AU. This can be understood with reference to Fig. 8 in which the balance of oxygen between CO and

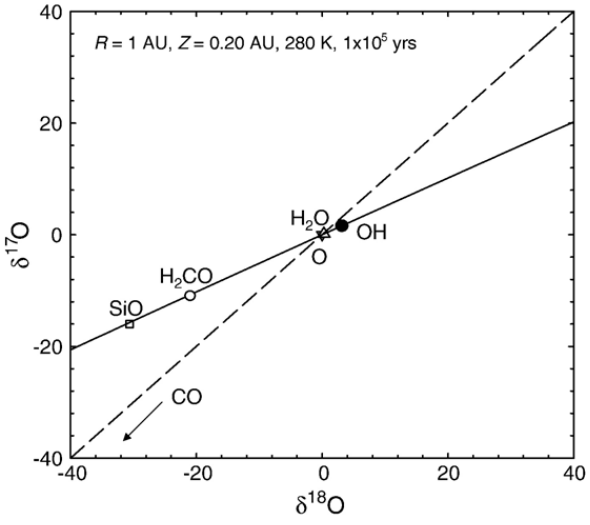

Fig. 7. Calculated time evolution of $\delta^{17}O$ and $\delta^{18}O$ in H_2O, O, OH, H_2CO, and SiO at $R=1.0$ AU and $Z=0.2$ AU in the static circumstellar disk model. The δ values are relative to the initial composition of the system. Rapid loss of CO (Fig. 5) precludes preservation of a non-mass dependent isotope effect due to CO photodissociation. The result is that oxygen-bearing species exhibit purely mass-dependent isotope effects. The mass-dependent fractionation curve (solid) and slope − 1.0 line (dashed) through the initial composition of the system are shown for reference.

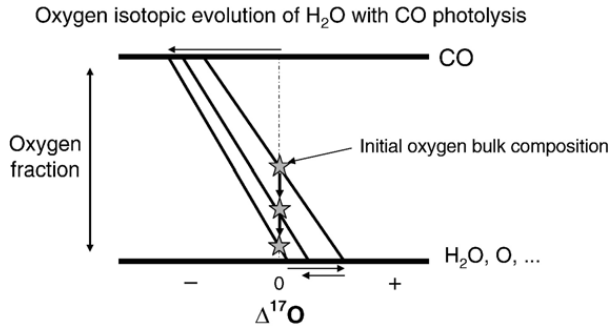

Fig. 8. Schematic diagram showing the influence of oxygen fraction (ordinate) on $\Delta^{17}O$ (abscissa) of reactant CO and product H_2O+O+ other subordinate O-bearing species during photodissociation of CO. Stars mark the bulk composition of the gas phase in terms of oxygen fractions of CO and H_2O+O+others at three different time steps. Black lines are tie lines connecting coexisting compositions of CO and H_2O+O+others. As CO is burned away, more and more oxygen is retained in H_2O+O and other O-bearing molecules. The net result is an initial rise in $\Delta^{17}O$ of H_2O+O that offsets the decrease in $\Delta^{17}O$ of residual CO, followed by a decrease in $\Delta^{17}O$ of product molecules, as shown in Fig. 5.

H_2O+O is shown schematically as photolysis of CO progresses. The initial condition of the system is one in which oxygen is partitioned subequally between CO and H_2O+O+others (others being subordinate in abundance to H_2O and O). As CO is destroyed a larger fraction of oxygen is present as H_2O+O+others. Eventually, as the oxygen fraction of CO becomes negligible, H_2O and O, now constituting the principal reservoirs of oxygen, return to the original isotopic composition of the system (Fig. 8). This process explains the loop traversed by H_2O in Fig. 5. If the rate of photodestruction of CO is too rapid in comparison to the redistribution of oxygen in the reaction network, product H_2O never experiences a significant increase in $\delta^{17}O$ and $\delta^{18}O$ because it is effectively always the dominant reservoir of O. In such cases, like that shown in Fig. 7 at $R=1$ AU, mass-dependent fractionation dominates over the isotopic effects of CO self shielding in species other than CO because of the rapid destruction of CO. This is why the isotopic effect of CO self shielding is an outer disk phenomenon. The caveat to this conclusion is that if the rate of CO delivery to the site of photodissociation was sufficient to replenish the rapidly dissociating CO, there would be no depletion in CO, but this becomes increasingly unlikely as the timescale for photodissociation approaches a year or less (e.g., Fig. 6).

5.2.1. Transport of H_2O to the inner Solar System

A major problem is the timescale over which oxygen isotope signals incurred in the outer regions of the solar nebula might have been transported to the region of terrestrial planet formation. The box model for the early Solar System (Fig. 3) can be used to show that high-$\Delta^{17}O$ H_2O could have entered the inner solar accretion disk in the region of rocky planet formation after approximately 10^5 yr.

In order to validate the box model approach, the original calculation of vertical mixing combined with CO self shielding presented by Lyons and Young is reproduced using the box model scheme shown in Fig. 3. For this calculation we adopted parameters analogous to those used by Lyons and Young (i.e., $k_{2-3}=k_{3-2}=5.5\times10^{-6}$ yr^{-1}, initial nH(2)/nH(3)$=10^{-5}$ where nH(i) refers to the number density of total hydrogen in reservoir i, and initial n(CO)/n(H)$=10^{-4}$, see Fig. 3) together with the effective rate constants for CO photodissociation indicated by the reaction network calculations here. The effective rate constant comes from the fact that CO photodestruction and H_2O formation reactions in disk surfaces can be approximated as a single reaction that converts CO to H_2O in the presence of H_2 with a rate constant k_{photo} of 10^{-5} yr^{-1} (Fig. 4). The reaction network calculations also indicate that the ratio of the effective rate constants for the ^{16}O and ^{18}O (^{17}O) isotopologues, e.g., $k_{photo}(^{16}O)/k_{photo}(^{18}O)$, is ~ 0.5 to 0.2 (this parameter is not unique, but varies, as shown in Fig. 5). The result (Fig. 9) shows that the box model approach is capable of capturing the essence of calculation schemes involving simultaneous solution of

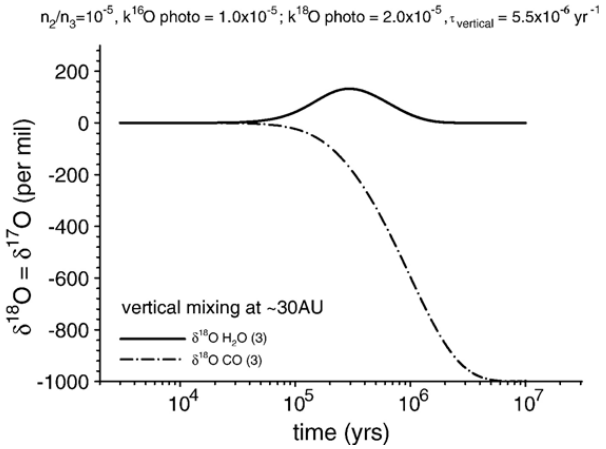

Fig. 9. Recalculation of the Lyons and Young (2005a) (L&Y) model for vertical mixing in the circumstellar disk at $R=30$ AU using the box model shown in Fig. 7. The result shows that the box model captures the essence of the mixing calculation of L&Y. The results are purposely plotted in a manner similar to that used by L&Y for comparison. The box model departs from the L&Y calculation in that δ values for CO drop to − 1000‰ (compared with − 600‰ in the L&Y calculation) and remain there because in this simplified model there is no mechanism for returning CO to the gas phase (the amount of CO returned in the L&Y model is relatively small).

equations for diffusion and reaction. The magnitude of the fractionation is identical to the original model when $k_{photo}(^{16}O)/k_{photo}(^{18}O)=0.5$.

Having shown that the box-model approach gives reasonable approximations to the problem of simultaneous CO photodissociation and vertical transport, we can expand its application to account for not only vertical mixing, but radial mixing as well. For this purpose our initial masses for the four reservoirs of interest relative to unit value of H_2O in reservoir (3) are: $H(1)=8.2\times10^5$ (the stellar H reservoir is effectively infinite, meaning any large value will suffice here), $H(2)=8.2\times10^{-3}$, $H(3)=8.2\times10^3$, and $H(4)=2.46\times10^2$. These values are based on spatial integrations of mass in the Kyoto disk model. In all cases initial $CO/H=10^{-4}$ and initial $H_2O/CO=1/2$. Note that this means there is considerable isotopically normal H_2O already in the inner portion of the disk prior to addition of ^{16}O-poor H_2O made in the outer disk.

Rate constants for transport in the box model are derived from the physics of disk evolution and stellar accretion as described in the literature. The vertical transport timescale is obtained from $k_{2-3}=k_{3-2}=\Omega\alpha=10^{-4}$ yr^{-1} where Ω is the mean orbital frequency and α is the alpha prescription for viscosity (Shakura and Sunyaev, 1973) (here $\Omega=1$ AU$/R^{3/2}$ was evaluated for a median outer disk R of 20 AU and $\alpha=10^{-2}$). Estimates of the timescale of inward radial transport in accretion disks yields $k_{3-4}=1\times10^{-5}$ yr^{-1} (Hartmann, 2000). Disk transport models indicate that water probably migrated primarily as ices condensed on larger grains and meter-sized boulders (Ciesla and Cuzzi, 2006; Cuzzi and Zahnle, 2004). In this way rates of radial transport of H_2O can exceed those of other species dominating the gas phase (e.g., H_2, O, CO). The box-model approach can account for such complexity by assigning different transport rate constants (e.g., k_{3-4}) to the different species of interest. Here we avoid this complication, however, in the interest of simplifying the interpretation of the results; we use a single rate constant for radial mixing for all species in the disk. In all cases a salient feature of transport will be more rapid vertical mixing than radial mixing. In future work the effects of more complicated radial transport models that decouple H_2O from other species should be explored, especially with reference to enhancement of H_2O relative to other gaseous species. We also include a return radial rate of transport equivalent to 1/10th the inward flow so that $k_{4-3}=k_{3-4}/10$. The latter accounts for lateral mixing and is consistent with observations of inner Solar System solid particles in comet Wild 2, for example (Brownlee et al., 2006). We used an intermediate stellar accretion rate of 10^{-7} $M_\odot$ yr^{-1}, yielding $k_{4-1}=10^{-7}$ yr^{-1} (the result is not sensitive to this rate within a factor of 10 or so).

From these input values one obtains the result shown in Fig. 10. The calculation shows a diachronous oxygen isotopic evolution across the disk with $\Delta^{17}O$ of H_2O rising first in the outer disk and later in the inner disk; the disk experiences a wave of high $\Delta^{17}O$ water passing from the outer disk to the inner disk on a timescale of 10^5 to 10^6 yr. The peak in time-dependent $\Delta^{17}O$ of the inner disk in this calculation is approximately twice the value implied for early inner Solar System water (Sakamoto et al., 2007). The precise magnitude of the peak $\Delta^{17}O$ value depends on the effective fractionation factor $k_{photo}(^{16}O)/k_{photo}(^{18}O)$ for the disk surface layers. For these calculations a conservative value of 0.22 was used.

The calculation summarized in Fig. 10 is for a closed system in which no CO is added to the surfaces of the disk. The model therefore applies to the disk after cessation of infall from the surrounding molecular cloud. An alternative calculation was performed (not shown) for which the amount of CO in the disk surface is in steady state, representing a balance between CO photodestruction and CO addition from the placental cloud (analogous to Eq. (8)). In this case $\Delta^{17}O$ of H_2O continues to rise unabated. Only when CO is no longer replenished by infall will $\Delta^{17}O$ of H_2O begin to fall again. In this circumstance the outer layers of the circumstellar disk act as factories for ^{16}O-depleted H_2O limited only by the duration of the infall phase.

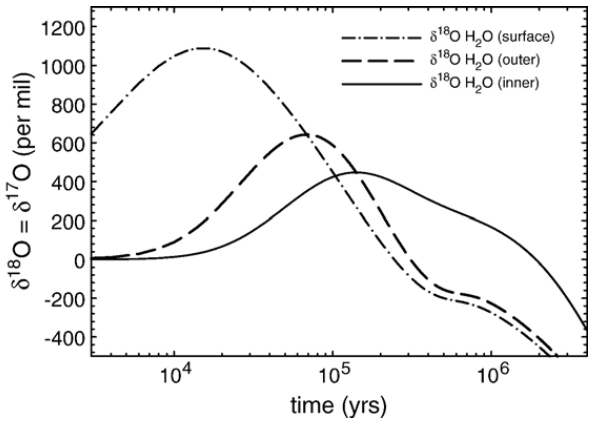

Fig. 10. Box model for $\delta^{18}O=\delta^{17}O$ evolution of H_2O in the solar circumstellar disk. $\Delta^{17}O$ is ~ 1/2 the $\delta^{18}O$ values shown. Curves show the time evolution of H_2O in the disk surfaces, outer disk, including the midplane, and the inner disk. The curves depict a wave of high $\Delta^{17}O$ values passing through the disk with time. Peak $\Delta^{17}O$ values arrive in the inner solar nebula at 10^5 yr and persist for up to 1 million years. The precise magnitude of the $\delta^{18}O=\delta^{17}O$ values depends on the fractionation factor used in the model, as described in the text.

Once ^{16}O-poor H_2O was produced in the region of CO self shielding it should have quickly frozen onto dust grain surfaces. Radial transport of these grains to the inner portions of the disk would ultimately have resulted in sublimation of the H_2O ice and increases in $\delta^{17}O$ and $\delta^{18}O$ of H_2O vapour there (Cuzzi and Zahnle, 2004; Young and Lyons, 2003). As described above, oxygen isotopic exchange between H_2O vapour and condensed silicate is known to be relatively efficient, unlike exchange between CO and melts, allowing for transfer of the ^{16}O-poor signal contained in water to silicate.

5.2.2. Comparisons with meteoritical data

Many observations are consistent with photodissociation of CO in the diffuse regions of the solar nebula as an explanation for the slope-1 line in oxygen isotope space. It accounts for the fact that H_2O was almost certainly depleted in ^{16}O (enriched in ^{18}O and ^{17}O, i.e., enriched in H_2Q) relative to silicates and other metal oxides in the Solar System. Production in the outer solar nebula also provides a natural explanation for the correlation between ^{16}O and the refractory nature of solids; many refractory minerals such as those found in CAIs should have retained their original ^{16}O-rich compositions because they would have had limited opportunity for reaction with H_2Q during transit through the nebula despite numerous heating events. Less refractory materials like Fe-bearing olivine and glass that comprise chondrite matrix, materials that are generally ^{16}O poor, had greater opportunity for exchange.

The assertion that exchange with H_2O is consistent with the oxygen isotope data for meteorites can be examined quantitatively with reference to self diffusion coefficients for oxygen in various pertinent mineral phases. The overall picture deduced from diffusivities of oxygen is one in which Fe-bearing dust and chondrules made from that dust exchanged with H_2O while important constituents of igneous CAIs did not exchange.

Self diffusion coefficients for Fe-bearing olivine, representing the less refractory dust in the solar nebula, and spinel, pyroxene and melilite, representing the more refractory CAIs, are known (Ryerson et al., 1989; Ryerson and McKeegan, 1994). These diffusivities can be compared by converting them into maximum radii of mineral grains that will experience complete oxygen isotope exchange for a given temperature and time. These maximum radii r_{max} are given by the expression (derived by rearranging Eq. (1) in Young et al. (2005))

$$r_{max} = \pi \left(\frac{-t(D_0 \exp(-E_a/(kT)))}{\ln(C/C_s)} \right)^{1/2} \quad (13)$$

where D_o is the preexponential for the diffusion coefficient, E_a is the activation energy for the diffusion coefficient, t is the duration for diffusion, and C/C_s is the ratio of concentration to the concentration imposed externally on the surface of the grain. Integrated heating times are thought to have been on the order of 10^2 to 10^3 years in the nebula (Shahar and Young, 2007; Simon et al., 2005; Young et al., 2005). For t=500 yr, C/C_s=0.1, and T=1600 K (a subsolidus temperature for both CAIs and olivine at nebular pressures) r_{max} values are 0.3 μm for olivine at appropriate fugacities of O_2, 22 μm for spinel, 3607 μm for melilite, and 130 μm for pyroxene. The r_{max} values can be compared with typical grain sizes of $\ll$ 1 μm for olivine in matrix, ~ 30 to 50 μm for spinel in igneous CAIs, $\geq$ 1000 μm or larger for melilite in igneous CAIs, and $\geq$ 500 μm for pyroxene in igneous CAIs. The comparison suggests that fine-grained sub-micron sized dust comprising matrix and precursors to CAIs both could have equilibrated with H_2O if given the opportunity. Matrix dust is ^{16}O poor, allowing for the interpretation that dust comprising matrix was indeed heated in the inner disk during passage of the ^{16}O-poor H_2O wave. CAIs, however, are generally ^{16}O rich and yet must have spent some time in the inner solar nebula where temperatures were high, suggesting that dust precursors to CAIs avoided being heated in the presence of ^{16}O-poor H_2O. This interpretation is consistent with early formation of CAIs prior to passage of the H_2O wave in the inner nebula. In the case of igneous CAIs made by partial melting, the r_{max} values predict that subsolidus heating of spinel and pyroxene in these CAIs should have retained their ^{16}O-rich compositions while melilite would not. Retention of ^{16}O-rich spinel and pyroxene would not have occurred if these mineral phases melted in the presence of ^{16}O-poor H_2O vapour because self diffusion of oxygen in liquids is rapid. However, spinel will not have entered the melt because it is the liquidus phase (the last solid phase to remain on the liquidus with heating) (Stolper and Paque, 1986). As a consequence, one would predict that spinels should have remained ^{16}O rich even after numerous partial melting events and indeed spinels in igneous CAIs are generally ^{16}O rich. Pyroxenes in CAIs will have melted near the CAI eutectic and preservation of ^{16}O-rich compositions in many, but not all, pyroxenes could imply some melting prior to (or after) the passage of the ^{16}O-poor wave of H_2O in the inner nebula.

These predictions are generally consistent with observations (Ryerson and McKeegan, 1994); igneous CAI spinel and pyroxene tend to be ^{16}O rich while igneous CAI melilite and the matrix of the meteorites are generally ^{16}O poor. The ^{16}O-poor compositions of chondrules are also consistent with this scenario because

dust similar to matrix was likely the precursor to chondrules. Melting of chondrules would have facilitated their exchange with H_2O gas due to the rapid self diffusion of O in silicate melt.

A slope of 1.0 on a plot of $\delta^{18}O$ vs. $\delta^{17}O$ is thought to represent the primordial oxygen reservoirs of the early solar system (Young and Russell, 1998). Any model for the ^{16}O variability in the Solar System should produce a similar slope. A slope-1 relation between $\delta^{18}O$ and $\delta^{17}O$ signifies variability in $^{16}O \gg {}^{18}O - {}^{17}O$. The first calculations by Lyons and Young (2005a) suggested a slope of 1.0 is to be expected as a product of CO self shielding but mass-dependent fractionation was not included in those calculations. The calculations presented here (e.g., Fig. 5 at $t > 150{,}000$ yr) suggest that a slope of 1.0 is produced even where some mass fractionation occurs. An important caveat is that we have included mass fractionation due to collisional frequencies but have not included zero-point energy and transition state bond rupture effects. As previously described, the latter effects can be large at low temperatures and more work is required to assess the full impact of mass-dependent fractionation on trends such as those shown in Fig. 5.

Transport times for the ^{16}O-poor H_2O produced in the models (Fig. 10) provide an arbiter for assessing the validity of the CO self shielding model if timescales for $^{16}O^{18}O_{-1}$ and $^{16}O^{17}O_{-1}$ exchange reactions in rocky materials of the Solar System can be deduced. Timescales for $\Delta^{17}O$ variation are not well known in the meteorite record as yet, in part because some oxygen isotope exchange occurred later on the meteorite parent bodies as well as in the disk itself. However, thermal processing of primitive materials like calcium–aluminium-rich inclusions and chondrules is thought to have lasted at least 10^5 yr (Young et al., 2005).

6. Conclusions

On the basis of these calculations one concludes that trapping of the CO self shielding isotopic effect, if it occurred, was an outer disk phenomenon. Inward radial transfer of high-$\Delta^{17}O$ H_2O produced by CO photolysis and self shielding would have taken place by virtue of a wave of high-$\Delta^{17}O$ H_2O that passed from disk surfaces through the outer disk and into the rocky planet-forming region on a timescale of 10^5 to 10^6 yr.

Acknowledgments

The author acknowledges support from the NASA Cosmochemistry program and the NASA Astrobiology Institute during the course of this study. Conversations about various aspects of this work with Pat Cassen and Edwin Schauble are gratefully acknowledged.

Appendix A. Supplementary Data

Supplementary data associated with this article can be found, in the online version, at doi:10.1016/j.epsl.2007.08.011.

References

Aikawa, Y., Herbst, E., 1999. Molecular evolution in protoplanetary disks. Astron. Astrophys. 351, 233–246.

Aikawa, Y., Herbst, E., 2001. Two-dimensional distributions and column densities of gaseous molecules in protoplanetary disks II. Deuterated species and UV shielding by ambient clouds. Astron. Astrophys. 371, 1107–1117.

Anders, E., Grevesse, N., 1989. Abundances of the elements: meteoritic and solar. Geochim. Cosmochim. Acta 53, 197–214.

Bally, J., Langer, W.D., 1982. Isotope-selective photodestruction of carbon monoxide. Astrophys. J. 255, 143–148.

Bergin, E., Calvet, N., Sitko, M., Abgrall, H., D'Alessio, P., Herczeg, G.J., Roueff, E., Qi, C., Lynch, D.K., Russell, R.W., Brafford, S.M., Perry, R.B., 2004. A new probe of the planet-forming region in T-Tauri disks. Astrophys. J. 614, L133–L136.

Bosenberg, J.S., Young, E.D., Ziegler, K., 2005. Evaporation and the absence of oxygen isotopic exchange between silicate melt and carbon monoxide gas at nebular pressures. 68th Annual Meteoritical Society Meeting, p. 5111.

Brittain, S.D., Rettig, T.W., Simon, T., Kulesa, C., 2005. CO line emission and absorption from the HL Tauri disk — where is all the dust? Astrophys. J. 626, 283–291.

Brownlee, D., Tsou, P., Aleon, J., Alexander, C.M.O.D., Araki, t., Bajt, S., Baratta, G.A., Bastien, R., Bland, P., Bleuet, P., Borg, J., Bradley, J.P., Brearley, A., Brenker, F., Brennan, S., Bridges, J.C., Browning, N.D., Brucato, J.R., Bullock, E., Burchell, M.J., Busemann, H., Butterworth, A., 2006. Comet 81P/Wild 2 under a microscope. Science 314, 1711–1716.

Caselli, P., Hasegawa, T.I., Herbst, E., 1998. A proposed modification of the rate equations for reactions on grain surfaces. Astrophys. J. 495, 309–316.

Choi, B., McKeegan, K.D., Krot, A.N., Wasson, J.T., 1998. Extreme oxygen-isotope compositions in magnetite from unequilibrated ordinary chondrites. Nature 392, 577–579.

Ciesla, F.J., Cuzzi, J.N., 2006. The evolution of the water distribution in a viscous protoplanetary disk. Icarus 181, 178–204.

Clayton, R.N., Mayeda, T.K., 1984. The oxygen isotope record in Murchison and other carbonaceous chondrites. Earth Planet. Sci. Lett. 67, 151–161.

Clayton, R.N., Grossman, L., Mayeda, T.K., 1973. A component of primitive nuclear composition in carbonaceous meteorites. Science 182, 458–488.

Cuzzi, J.N., Zahnle, K.J., 2004. Material enhancement in protoplanetary nebulae by particle drift through evaporation fronts. Astrophys. J. 614, 490–496.

Dubey, M.K., Mohrschladt, R., Donahue, N.M., Anderson, J.G., 1997. Isotope specific kinetics of hydroxyl radical (OH) with water (H_2O): testing models of reactivity and atmospheric fractionation. J. Phys. Chem. 101, 1494–1500.

Fagan, T.J., Krot, A.N., Keil, K., Yurimoto, H., 2004. Oxygen isotopic evolution of amoeboid olivine aggregates in the reduced CV3 chondrites Efremovka, Vigarano, and Leoville. Geochim. Cosmochim. Acta 68, 2591–2611.

Fegley, B., 2000. Kinetics of gas-grain reactions in the solar nebula. Space Sci. Rev. 92, 177–200.

Glassgold, A.F., Feigelson, E.D., Montmerle, T., Wolk, S., 2005. X-ray flares of sun-like young stellar objects and their effects on protoplanetary disks. In: Krot, A.N., Scott, E.R.D., Reipurth, B. (Eds.), Chondrites and the Protoplanetary Disk. Astronomical Society of the Pacific, pp. 165–180.

Greenblatt, G.D., Howard, C.J., 1989. Oxygen atom exchange in the interaction of 18OH with several small molecules. J. Phys. Chem. 93, 1035–1042.

Hartmann, L., 2000. Observational constraints on transport (and mixing) in pre-main sequence disks. Space Sci. Rev. 92, 55–68.

Hasegawa, T.I., Herbst, E., Leung, C.M., 1992. Models of gas-grain chemistry in dense interstellar clouds with complex organic molecules. Astrophys. J., Suppl. Ser. 82, 167–195.

Herbst, E., 2000. The astrochemistry of H_3^+. Philos. Trans. R. Soc. Lond., 358, 2523–2534.

Jaffe, S., Klein, F.S., 1966. Isotopic exchange reactions of atomic oxygen produced by the photolysis of NO2 at 3660 A. Trans. Faraday Soc. 62, 3135–3141.

Jura, M., 1974. Formation and destruction rates of interstellar H_2. Astrophys. J. 191, 375–379.

Kamp, I., Bertoldi, F., 2000. CO in the circumstellar disks of Vega and b Pictoris. Astron. Astrophys. 353, 276–286.

Kenyon, S.J., Hartmann, L., 1987. Spectral energy distributions of T Tauri stars: disk flaring and limits on accretion. Astrophys. J. 323, 714–733.

Langer, W.D., Graedel, T.E., Frerking, M.A., Armentrout, P.B., 1984. Carbon and oxygen isotope fractionation in dense interstellar clouds. Astrophys. J. 277, 581–604.

Lasaga, A.C., 1980. The kinetic treatment of geochemical cycles. Geochim. Cosmochim. Acta 44, 815–840.

Le Teuff, Y.H., Millar, T.J., Markwick, A.J., 2000. The UMIST database for astrochemistry 1999*. Astron. astrophys., Suppl. Ser. 146, 157–168.

Lee, H.H., Herbst, E., desForets, G.P., Roueff, E., LeBourlot, J., 1996. Photodissociation of H_2 and CO and time dependent chemistry in inhomogeneous interstellar clouds. Astron. Astrophys. 311, 690–707.

Liang, M.C., Blake, G.A., Yung, Y.L., 2004. A semianalytic model for photo-induced isotopic fractionation in simple molecules. J. Geophys. Res. 109, D10308. doi:10.1029/2004JD004539.

Lyons, J.R., Young, E.D., 2005a. CO self-shielding as the origin of oxygen isotope anomalies in the early solar nebula. Nature 435 (7040), 317–320.

Lyons, J.R., Young, E.D., 2005b. Evolution of oxygen isotopes in the solar nebula. Nature 435, 317–320.

Maruyama, S., Yurimoto, H., Sueno, S., 1999. Oxygen isotope evidence regarding the formation of spinel-bearing chondrules. Earth Planet. Sci. Lett. 169, 165–171.

Melendez, J., 2004. A low solar oxygen abundance from the first-overtone OH lines. Astrophys. J. 615, 1042–1047.

Miller, C.E., Yung, Y.L., 2000. Photo-induced isotope fractionation. J. Geophys. Res. 105, 29039–29051.

Prieto, C.A., Lambert, D.L., Asplund, M., 2002. A reappraisal of the solar photospheric C/O ratio. Astrophys. J. 573, L137–L140.

Ryerson, F.J., McKeegan, K.D., 1994. Determination of oxygen self-diffusion in åkermanite, anorthite, diopside, and spinel: implications for oxygen isotopic anomalies and the thermal histories of Ca–Al-rich inclusions. Geochim. Cosmochim. Acta 58, 3713–3734.

Ryerson, F.J., Durham, W.B., Cherniak, D.J., Lanford, W.A., 1989. Oxygen diffusion in olivine: effect of oxygen fugacity and implications for creep. J. Geophys. Res. 94, 4105–4118.

Sakamoto, N., Seto, Y., Itoh, S., Kuramoto, K., Fujino, K., Nagashima, K., Krot, A.N., Yurimoto, H., 2007. Remnants of early Solar System water enriched in heavy oxygen isotopes. Science 317, 231–233.

Shahar, A., Young, E.D., 2007. Astrophysics of CAI formation as revealed by silicon isotope LA-MC-ICPMS of an igneous CAI. Earth Planet. Sci. Lett. 257, 497–510.

Shakura, N.I., Sunyaev, R.A., 1973. Black holes in binary systems. Observational appearance. Astron. Astrophys. 24, 337–355.

Sheffer, Y., Lambert, D.L., Federman, S.R., 2002. Ultraviolet detection of interstellar 12C17O and the CO isotopomeric ratios toward X Persei. Astrophys. J. 574, L171–L174.

Shu, F.H., Shang, H., Lee, T., 1996. Toward an astrophysical theory of chondrites. Science 271, 1545–1552.

Simon, J.I., Young, E.D., Russell, S.S., Tonui, E.K., Dyl, K.A., Manning, C.E., 2005. A short timescale for changing oxygen fugacity in the solar nebula revealed by high-resolution ^{26}Al–^{26}Mg dating of CAI rims. Earth Planet. Sci. Lett. 238 (3–4), 272–283.

Stolper, E.M., Paque, J.M., 1986. Crystallization sequences of Ca–Al-rich inclusions from Allende: the effects of cooling rate and maximum temperature. Geochim. Cosmochim. Acta 50, 1785–1806.

van Dishoeck, E., Black, J.H., 1988. The photodissociation and chemistry of interstellar CO. Astrophys. J. 334, 771–802.

Wasson, J.T., Rubin, A.E., Yurimoto, H., 2004. Evidence in CO3.0 chondrules for a drift in the O isotopic composition of the solar nebula. Meteorit. Planet. Sci. 39, 1591–1598.

Willacy, K., Langer, W.D., 2000. The importance of photoprocessing in protoplanetary disks. Astrophys. J. 544, 903–920.

Willacy, K., Klahr, H.H., Millar, T.J., Henning, T., 1998. Gas and grain chemistry in a protoplanetary disk. Astron. Astrophys. 338, 995–1005.

Wilson, T.L., 1999. Isotopes in the interstellar medium and circumstellar envelopes. Rep. Prog. Phys. 62, 143–185.

Yang, M., Zhang, D.H., Collins, M.A., Lee, S.-Y., 2001. Ab initio potential-energy surfaces for the reaction $OH+H_2=H_2O+H$. J. Chem. Phys. 115, 174–178.

Yoshitake, M., Koide, Y., Yurimoto, H., 2005. Correlations between oxygen-isotopic composition and petrologic settings in a coarse-grained Ca, Al-rich inclusion. Geochim. Cosmochim. Acta 69, 2663–2674.

Young, E.D., 2001. The hydrology of carbonaceous chondrite parent bodies and the evolution of planet progenitors. Philos. Trans. R. Soc. Lond., A 359, 2095–2110.

Young, E.D., 2007. Strange water in the Solar System. Science 317, 211–212.

Young, E.D., Ash, R.D., England, P., Rumble, D., 1999. Fluid flow in chondritic parent bodies: deciphering the compositions of planetesimals. Science 286 (5443), 1331–1335.

Young, E.D., Lyons, J.R., 2003. CO self shielding in the outer solar nebula: an astrochemical explanation for the oxygen isotope slope-1 line. Lunar and Planetary Science Conference, vol. XXXIV, p. 1923.

Young, E.D., Russell, S.S., 1998. Oxygen reservoirs in the early solar nebula inferred from an Allende CAI. Science 282, 452–455.

Young, E.D., Simon, J.I., Galy, A., Russell, S.S., Tonui, E., Lovera, O., 2005. Supra-canonical Al-26/Al-27 and the residence time of CAIs in the solar protoplanetary disk. Science 308 (5719), 223–227.

Yu, Y., Hewins, R.H., Clayton, R.N., Mayeda, T.K., 1995. Experimental study of high temperature oxygen isotope exchange during chondrule formation. Geochim. Cosmochim. Acta 59, 2095–2104.

Yurimoto, H., Kuramoto, K., 2002. A possible scenario introducing heterogeneous oxygen isotopic distribution in protoplanetary disks. 65th Meteoritical Society, p. 5149.

Yurimoto, H., Ito, M., Nagasawa, H., 1998. Oxygen isotope exchange between refractory inclusion in Allende and solar nebula gas. Science 282, 1874–1877.

Yurimoto, H., Kuramoto, K., 2004. Molecular cloud origin for the oxygen isotope heterogeneity in the solar system. Science 305, 1763–1766.